Elavl2 Regulates Retinal Function Via Modulating the Differentiation of Amacrine Cells Subtype

Mengjuan Wu,[1] Qinqin Deng,[1] Xinlan Lei,[1] Yuxin Du,[1] and Yin Shen[1,2]

[1]Eye Center, Renmin Hospital of Wuhan University, Wuhan University, Wuhan, Hubei, China
[2]Frontier Science Center for Immunology and Metabolism, Medical Research Institute, School of Medicine, Wuhan University, Wuhan, Hubei, China

Correspondence: Yin Shen, Eye Center, Renmin Hospital of Wuhan University, Wuhan University, Wuhan 430060, Hubei, China; Frontier Science Center for Immunology and Metabolism, Medical Research Institute, School of Medicine, Wuhan University, Wuhan 430071, Hubei, China;
yinshen@whu.edu.cn.

MW and QD contributed equally to this work.

Received: December 16, 2020
Accepted: May 6, 2021
Published: June 1, 2021

Citation: Wu M, Deng Q, Lei X, Du Y, Shen Y. Elavl2 regulates retinal function via modulating the differentiation of amacrine cells subtype. *Invest Ophthalmol Vis Sci.* 2021;62(7):1. https://doi.org/10.1167/iovs.62.7.1

Purpose. The neuronal ELAV-like proteins (nElavls; Elavl2, Elavl3, Elavl4) have been known to regulate neuronal differentiation, maintenance, and axonogenesis in the brain. However, the specific role of nElavls in retina remains unclear. Here, we attempted to identify the expression pattern of Elavl2 during retinogenesis and aimed to decipher the function of Elavl2 in the retina.

Methods. We have used the Cre-*loxP* system to conditionally inactivate *Elavl2* in order to examine its role in developing retina. Eyes were collected for histology, immunohistochemistry, and TUNEL analysis to identify the structure of retina, and examined by RNA sequencing to analyze the function and pathway enrichment of differentially expressed genes in transgenic mice. Moreover, the mechanism by which Elavl2 regulates the differentiation of amacrine cells (ACs) was explored by RNA immunoprecipitation assays. Finally, eyes were functionally assessed by whole-cell patch-clamp, electroretinography (ERG) and optomotor response.

Results. Elavl2 was expressed in retinal progenitor cells and retinal ganglion cells (RGCs), ACs, and horizontal cells. Retina-specific ablation of *Elavl2* led to the loss of ACs and the transcription factors involved in ACs differentiation were also downregulated. In addition, the spontaneous activities of RGCs were obviously increased in *Elavl2*-deficient mice. Meanwhile, the loss of ACs that induced by *Elavl2* deficiency lead to a decrease in ERG responses and visual acuity.

Conclusions. Elavl2 is an intrinsic factor that involved in the differentiation of ACs subtype during retinogenesis, and essential for maintaining the normal retinal function.

Keywords: Elavl2, amacrine cells, retinal development, transcription factor, retinal function

The neuronal ELAV-like proteins (nElavls) are highly rich in neurons[1] and play an important role in multiple steps of neuronal development associated with neuronal differentiation, maintenance, axonogenesis, and synaptic plasticity through their direct binding to the sequence of target mRNA in an activity-dependent manner or at a steady-state level.[2–4] Elavl2 (ELAV-like neuron-specific RNA-bp2) is a member of the nElavls family and identified as autoimmune antigens in a multisystem neurologic disorder in patients with paraneoplastic encephalomyelopathy.[5] In the embryonic forebrain, Elavl2 completely restores the miR-9-dependent gene silencing of Foxg1, a critical transcriptional factor (TF) in the central nervous system.[6] Moreover, the expression of Tbr2, a marker for intermediate basal neuronal progenitor cells, is partly colabeled with Elavl2 protein during cortical development, indicating the specific functions of Elavl2 in the division of neurons.[7]

The retina is a part of the central nervous system derived from the forebrain neural ectoderm.[8] Amacrine cells (ACs) are the important inhibitory intermediate neurons in the retina that could regulate visual information to RGCs, enabling elaborate visual functions. At present, there are more than 60 subtypes of ACs in the retina.[9] Despite their broad morphological diversity, ACs are often divided into three groups, including GABAergic ACs, glycinergic ACs, and non-GABAergic–non-glycinergic ACs, based on the expression of neurotransmitters. Although all types of ACs are generated from the multipotent retinal progenitor cells, they subsequently differentiate into different subtypes after combined action of the intrinsic and extrinsic factors during retinogenesis.[10–12] TFs are commonly used as the critical intrinsic components to regulate the cytogenesis, maintenance, and cell fate determination of retinal progenitors.[10] For instance, Foxn4 is required by retinal progenitor cells for the amacrine and horizontal precursors at early stages of retinogenesis.[13,14] Ptf1a has been shown to coordinate with the Prdm13 and together regulate the balance of inhibitory and excitatory neurons.[15,16] During retinogenesis, deficiency of *Prdm13* leads to a significant decrease in the number of CALBs$^+$ GABAergic or glycinergic ACs,[17] together with the Ebf3$^+$ ACs.[18] In addition, Barhl2 has been verified to play an important role in specifying both glycinergic and GABAergic ACs[19,20]; meanwhile, Nr4a2 and Pax6 are involved in specifying GABAergic and glycinergic ACs, respectively.[21,22]

Disruption in the balance of TFs including Six6, Vax1, Vsx2 or Otx2, could result in aberrant retinal development and retinal dysfunction, as well as microphthalmia.[23] Currently, the molecular mechanism of governing the specification or differentiation of ACs remains elusive.

Here, we characterize the expression profile and localization of Elavl2, and explore the role of it in the developing and adult mouse retina. Furthermore, our studies reveal the differences of the generation of ACs in *Elavl2*-deficient retina, and their effects on the RGCs activities and normal visual functions. On the basis of these observations, our findings highlight a novel role for Elavl2 signaling in the retina.

Methods

Animals

All procedures were performed according to the National Institutes of Health guidelines and approved by the Wuhan University Laboratory Animal Center and compiled with the ARVO statement for the Use of Animals in Ophthalmic and Vision Research. To generate a floxed *Elavl2* allele, we inserted loxP sites in introns 5 and 6 by homologous recombination (Fig. 3A). Conditional knock-out mice were obtained by crossing floxed *Elavl2* allele mice with the Six3-Cre transgenic line to delete exon 5 of *Elavl2* in the developing retina to produce the $Elavl2^{fl/fl}$, $Elavl2^{fl/+}$; *Six3-Cre* and $Elavl2^{fl/fl}$; *Six3-Cre* ($Elavl2^{\Delta fl/\Delta fl}$) mice, and maintained by breeding with C57BL6/J (wild type) mice.

Immunohistochemistry

Retinal sections were blocked with a mixture of 2% bovine serum albumin (BSA) and 0.1% Triton-X-100 in PBS for one hour at room temperature (RT). At the end of the blocking, the sections were incubated overnight at 4°C with primary antibodies (Supplementary Table S1) and secondary antibodies for one hour, followed by 4',6-diamidino-2-phenylindole (DAPI) for nuclear staining and imaging under the confocal Olympus FV1000 laser scanning microscope (Olympus, Tokyo, Japan).

RNA Sequencing (RNA-seq) Analysis

Total RNA was isolated from Postnatal (P) 6 retinas of $Elavl2^{fl/fl}$ and $Elavl2^{\Delta fl/\Delta fl}$ mice using TRIzol Reagent (Invitrogen) according to the manufacturer's instruction. 2 µg RNA was used for library preparation using KCTM Stranded mRNA Library Prep Kit for Illumina (Wuhan Seqhealth Co., Ltd., Wuhan, China) and sequencing with Novaseq 6000 sequencer with PE150 model (Illumina, San Diego, CA, USA). The obtained sequence reads were first filtered by Trimmomatic.[24] Clean data were mapped to the reference genome of mouse from ftp://ftp.ensembl.org/pub/release-87/fasta/mus_musculus/dna/ using STRA software with default parameters.[25] Reads mapped to the exon regions of each gene were counted by featureCounts (Subread-1.5.1; Bioconductor) and then reads per kilobase per million reads were calculated.[26] A *P*-value cutoff of 0.05 and fold-change cutoff of 2 were used to judge the statistical significance of gene expression differences. The heatmap and scatter plots were performed using the R software package. Gene ontology analysis and Kyoto encyclopedia of genes and genomes (KEGG) enrichment analysis for the differentially expressed genes were both implemented by KOBAS software.[27]

Real-Time Quantitative Reverse Transcription (qRT)-PCR

After euthanizing mice, total RNA was quickly extracted from different genotypes retinas using the TRIzol reagent (Invitrogen, Carlsbad, CA, USA). The gene transcription was quantified by qRT-PCR with SYBR Green I fluorescent dye (Vazyme Biotech Co., Ltd, Nanjing, China). All values were calibrated relative to the endogenous levels of *Gapdh* and normalized to that of the control group. The primers used for qRT-PCR were described in Supplementary Table S2.

TUNEL Assay

Terminal deoxynucleotidyl transferase dUTP nick end labeling (TUNEL) in situ labeling was performed on retinal cryosections using One Step TUNEL Apoptosis Assay Kit (Beyotime Biotechnology, Jiangsu, China) according to the manufacturer's instruction. Briefly, retinal sections were incubated with 0.5% Triton-X-100 in PBS for five minutes at RT after washed with PBS, and then incubated one hour at 37°C with TUNEL detection solution, followed by DAPI for nuclear staining and imaging under the Olympus FV1000 confocal laser scanning microscope.

RNA Immunoprecipitation (RIP) Assay

For RIP assay, protein A/G magnetic beads (Thermo Fisher Scientific, USA) were incubated with antibody against Elavl2 or normal IgG for two hours and followed by the incubated with retina extracts at 4°C overnight. After washing, 200 µL TE buffer containing 10 mM DTT was used to elute protein and RNA complexes for 30 minutes at 37°C. The enriched RNAs were then extracted by TRIzol and analyzed by qRT-PCR.

Electroretinogram (ERG)

ERG responses were recorded in P30, P120 and P270 $Elavl2^{\Delta fl/\Delta fl}$ and the control mice using the RetiMINER IV system (IRC Medical Equipment, Chongqing, China) just as performed previously.[28] After adaption to darkness, scotopic ERGs were recorded at stimulus intensities levels of 0.003, 0.01, 0.03, 0.1, 0.3, 1.0, 3.0, 10 cd. s/m^2, with 30-second intervals. Oscillatory potentials (OPs) were recorded using the white flashes of 3.0 cd. s/m^2 scotopic responses via band-pass filtering between 50 and 170 Hz.

Optomotor Response (OMR)

To evaluate the visual acuity of mice, OMR recordings were carried out as reported previously.[29] Briefly, OMR recordings in P30 and P120 $Elavl2^{\Delta fl/\Delta fl}$ and the control mice were collected under the same conditions. After darkness adaptation, mice were tested freely on a platform in the center of a box, which consisted of four identical sizes of LED screens displaying revolving vertical black and white stripes (Fig. 8C). Ten spatial frequencies, including 0.1, 0.15, 0.2, 0.25, 0.3, 0.35, 0.4, 0.45, 0.5, and 0.6 cycles/deg were gradually tested. The movements of mice were videotaped using an infrared camera placed above the chamber to calculate the number of head tracking movements during each spatial frequency.[30]

Investigative Ophthalmology & Visual Science

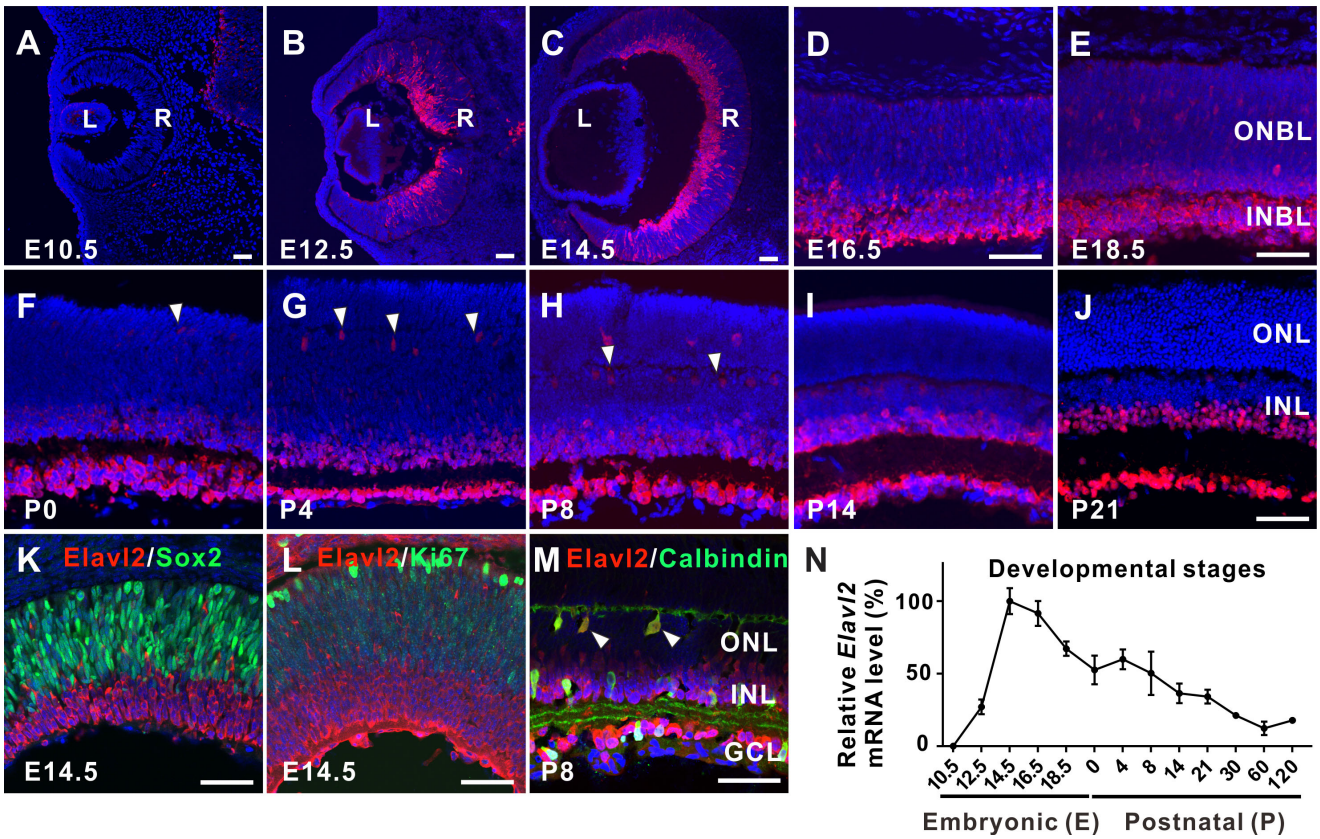

Figure 1. The spatiotemporal expression patterns of Elavl2 in developing retina. **(A–J)** The retinal sections were double-immunostained with an anti-Elavl2 antibody (red) and DAPI (blue) from wild type mice at the presented developmental time points. Arrowheads indicate the migrating HCs. **(K, L)** Sections from embryonic (*E*) 14.5 mouse retinas were stained with DAPI (*blue*) and co-labeled with anti-Elavl2 antibody (*red*), and anti-Sox2 antibody (*green*) **(K)**, anti-Ki67 antibody (*green*) **(L)**. **(M)** The sections were stained with DAPI and co-labeled with anti-Elavl2 antibody (*red*) and anti-Calbindin antibody (*green*). **(N)** Temporal expression levels of *Elavl2* from E10.5 to adult stages during retinal development was determined by qRT-PCR analysis, and presented as percentages relative to the highest samples, with error bars representing standard error of the mean (SEM, n $\geq$ 3). R, retina; L, lens; INBL, inner neuroblast layer; ONBL, outer neuroblast layer; ONL, outer nuclear layer. *Scale bar*: 50 µm.

Whole-Cell Patch-Clamp Recordings

Whole-cell patch-clamp recordings were carried out as previously reported.[31] Briefly, after adaptation to darkness, mice were anesthetized with isoflurane and were softly dissected the neural retinas. After the dissection, the retinas were quickly transferred to the adjacent recording chamber. To maintain the activity of RGCs, the retina were always kept submerged in Ringer's solution containing 125 mM NaCl, 2.5 mM KCl, 1 mM $MgSO_4$, 2 mM $CaCl_2$, 1.25 mM NaH_2PO_2, 26 mM $NaHCO_3$, and 20 mM glucose, with pH adjusted to 7.3 using NaOH and bubbled with 95% O_2/5% CO_2. Before recording, the prepared retinas were continually left to adapt to the darkness for 30 minutes at 26° to 28°C. The spontaneous action potentials of RGCs were obtained under current-clamp with a Multiclamp 700B amplifier (Axon Instrument) at 10 kHz and filtered at 2 kHz for three minutes. Electrodes (resistances of 5–7 MΩ) were fabricated from borosilicate glass using a four-stage Horizontal puller (PC-10; Narishige, Tokyo, Japan) and filled with an intracellular solution composed of 120 mM K-gluconate, 0.1 mM $CaCl_2$, 1 mM $MgCl_2 \cdot 6H_2O$, 1 mM EGTA, 10 mM HEPES, 4 mM ATP-Mg, 0.3 mM GTP-Na_2, and 10 mM phosphocreatine Tris, with pH adjusted to 7.3 using KOH. Data acquisitions were recorded and analyzed using the Patchmaster and Mini Analysis Program, respectively. Data were excluded if an RGC did not show a spontaneous action for a minimum of three minutes during recording.

Experimental Design and Statistical Analysis

All measurements were analyzed by individuals blinded to the experiment. For quantitative analysis, data were displayed as the mean ± SEM. Significances between two groups were examined using the Student's t-test (SPSS15.0.1; SPSS, Inc., Chicago, IL, USA). $P < 0.05$ was considered statistically significant.

Results

Pattern of Elavl2 Expression During Retinal Development

In the nElavl family, Elavl3 and Elavl4 have been identified as specific cell markers for the early differentiation of RGCs and ACs in zebrafish.[32] We performed immunofluorescent staining to explore the spatial and temporal expression pattern of Elavl2 in mouse retina. Beginning in neuroblastic cells, Elavl2 was observed as early as embryonic (E) 12.5 in retina (Figs. 1A, 1B). Followed by a dynamically changing pattern,

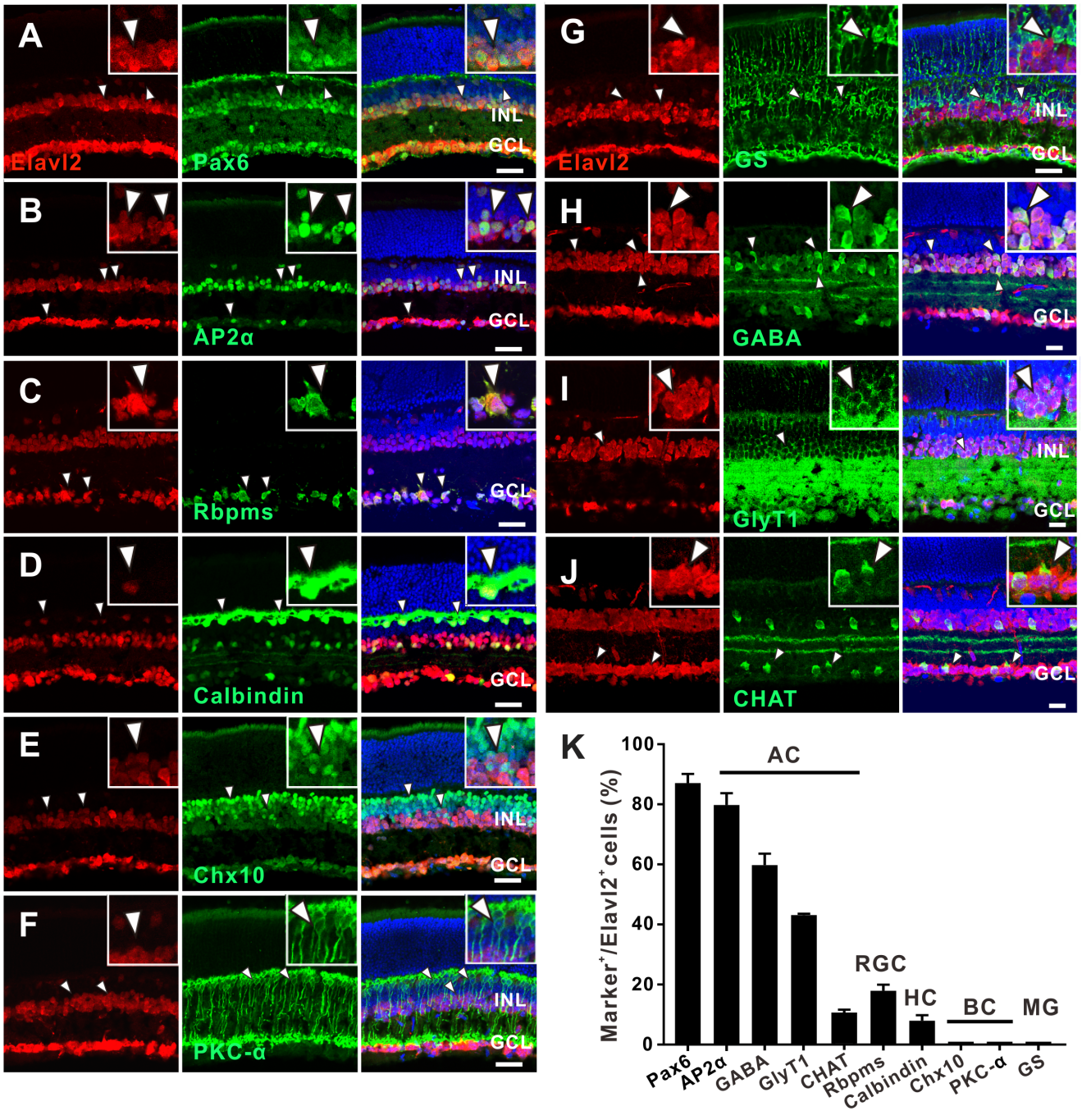

Figure 2. Co-label immunofluorescence illustrating colocalization of Elavl2 in the retina at P14. **(A–J)** The retinal cross-sections at P14 were stained with DAPI (*blue*) and co-labeled with anti-Elavl2 (*red*) and the following markers: Pax6 for RGCs, ACs and HCs **(A)**, AP2*α* for pan-ACs **(B)**, Rbpms for RGCs **(C)**, Calbindin for HCs **(D)**, Chx10 for BCs **(E)**, PKC-*α* for on-bipolar cells **(F)**, GS for Müller cells **(G)**, GABA for GABAergic ACs **(H)**, GlyT1 for glycinergic ACs **(I)**, CHAT for cholinergic ACs **(J)**. Arrowheads indicate representative the colocalized cells and insets show the higher magnification of corresponding regions. (K) Quantification of specific marker-positive retinal cells those are immunoreactive for Elavl2 at P14. Results are presented as the mean ± SEM (n ≥ 3). RGC, retina ganglion cell; HC, horizontal cell. *Scale bar*: 50 µm.

Elavl2 was restricted to the inner neuroblastic layers (INBL) and few migrating cells in the outer neuroblastic layers (ONBL) (Figs. 1B–1G), suggesting Elavl2 may be expressed in postmitotic cells at this stage. Consistently, very few Elavl2 co-expressed with Sox2 or Ki67, which was expressed by retinal progenitors or proliferation cells respectively[33] (Figs. 1K, 1L). From P8 to mature retinas (Figs. 1H–1J), Elavl2 gradually confined to the ganglion cell layer and innermost region of the inner nuclear layer (INL) where the RGCs and ACs are located, as well as the outer migrating horizontal cells (HCs) (Fig. 1M, Supplementary Fig. S1). Therefore Elavl2 is transiently expressed in INBL, and then essentially limited to the inner retina as development progresses. Additionally, Elavl2 mRNA was highly expressed in embryonic

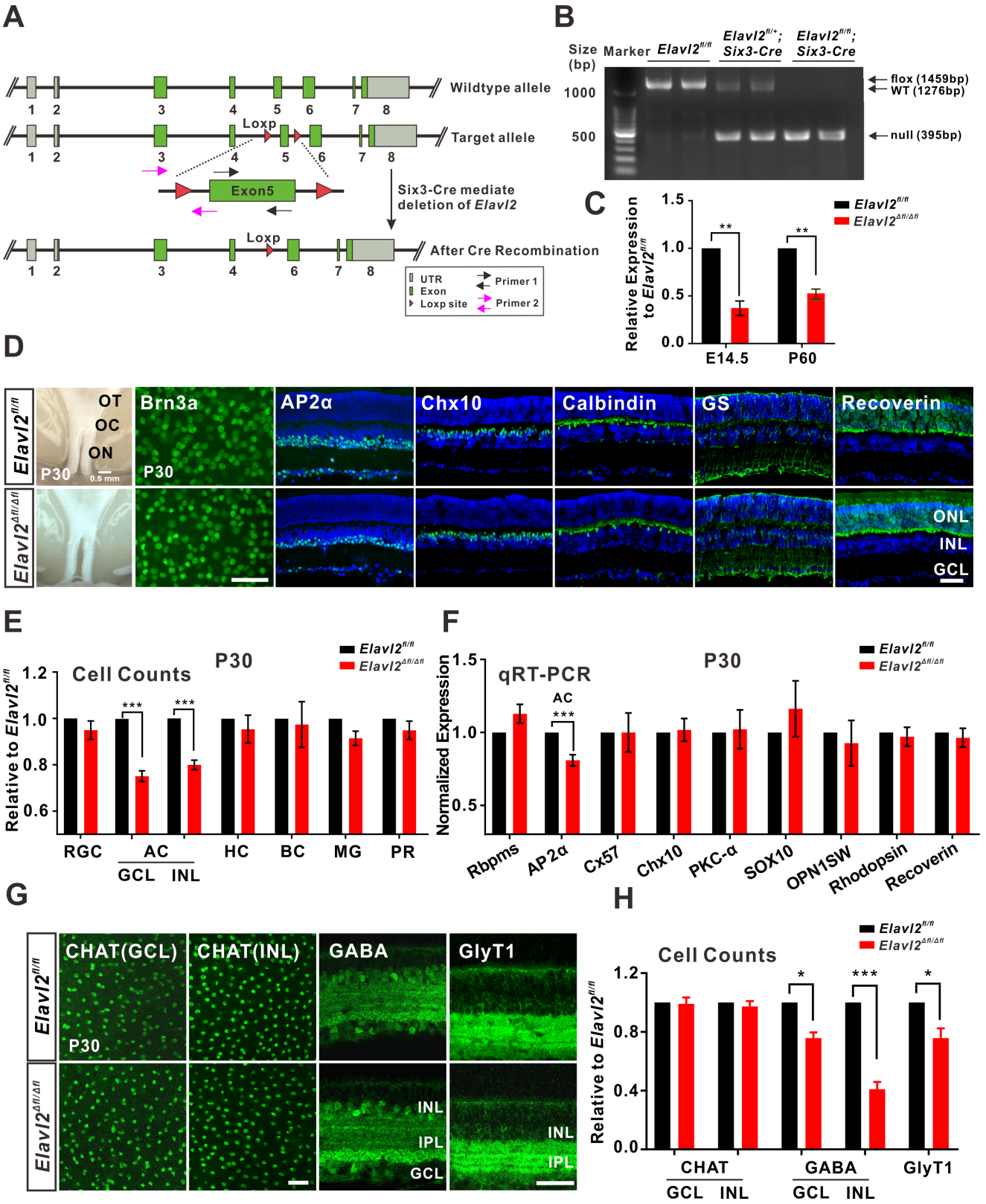

Figure 3. *Elavl2* deficiency results in a specific loss of ACs in adult retina. **(A)** A floxed *Elavl2* mouse line was bred with the Six3-Cre transgenic mice to conditionally delete exon 5 of *Elavl2* in the developing retina. **(B)** All the genotypes (*Elavl2*$^{fl/fl}$, *Elavl2*$^{fl/+}$;*Six3-Cre* and *Elavl2*$^{fl/fl}$;*Six3-Cre*) were determined by PCR. **(C)** Decreased expression of *Elavl2* in the *Elavl2*-deficient retina. Results are presented as the fold expression relative to *Elavl2*$^{fl/fl}$ littermates, with error bars representing standard error of the mean (SEM, n ≥ 3). **(D)** Immunostaining of retinal sections or whole-mounts at P30 from *Elavl2*$^{fl/fl}$ and *Elavl2*$^{\Delta fl/\Delta fl}$ mice were double-immunostained with antibodies against specific cell markers (*green*) and DAPI (*blue*). *Scale bar*: 50 µm. **(E)** Quantitation of the retinal cells for each specific marker per retina section, except that Brn3a^{+} cells were counted per area of retinal flat-mounts. Results are presented as the mean ± SEM (n ≥ 3) and normalized to *Elavl2*$^{fl/fl}$

Investigative Ophthalmology & Visual Science

littermates. **(F)** The expression of the selected retinal cell-related genes at P30 in *Elavl2*$^{fl/fl}$ and *Elavl2*$^{\Delta fl/\Delta fl}$ retinas were determined by qRT-PCR analysis, and normalized to *Elavl2*$^{fl/fl}$ littermates. **(G)** Immunostaining of whole-mounts or retinal sections at P30 from *Elavl2*$^{fl/fl}$ and *Elavl2*$^{\Delta fl/\Delta fl}$ mice with antibodies against the indicated markers (*green*). *Scale bar*: 50 µm. **(H)** Quantitation of the retinal cells for each specific marker per retina section, except that CHAT^{+} cells were counted per area of retinal flat-mounts. Results are presented as the mean ± SEM (n ≥ 3) and normalized to *Elavl2*$^{fl/fl}$ littermates. Asterisks indicate statistically significant differences between *Elavl2*$^{fl/fl}$ and *Elavl2*$^{\Delta fl/\Delta fl}$ mice (*P < 0.05, **P < 0.01, ***P < 0.001). OT, optic tract; OC, optic chiasm; ON, optic nerve; ONL, outer nuclear layer; IPL, inner plexiform layer; GCL, ganglion cell layer.

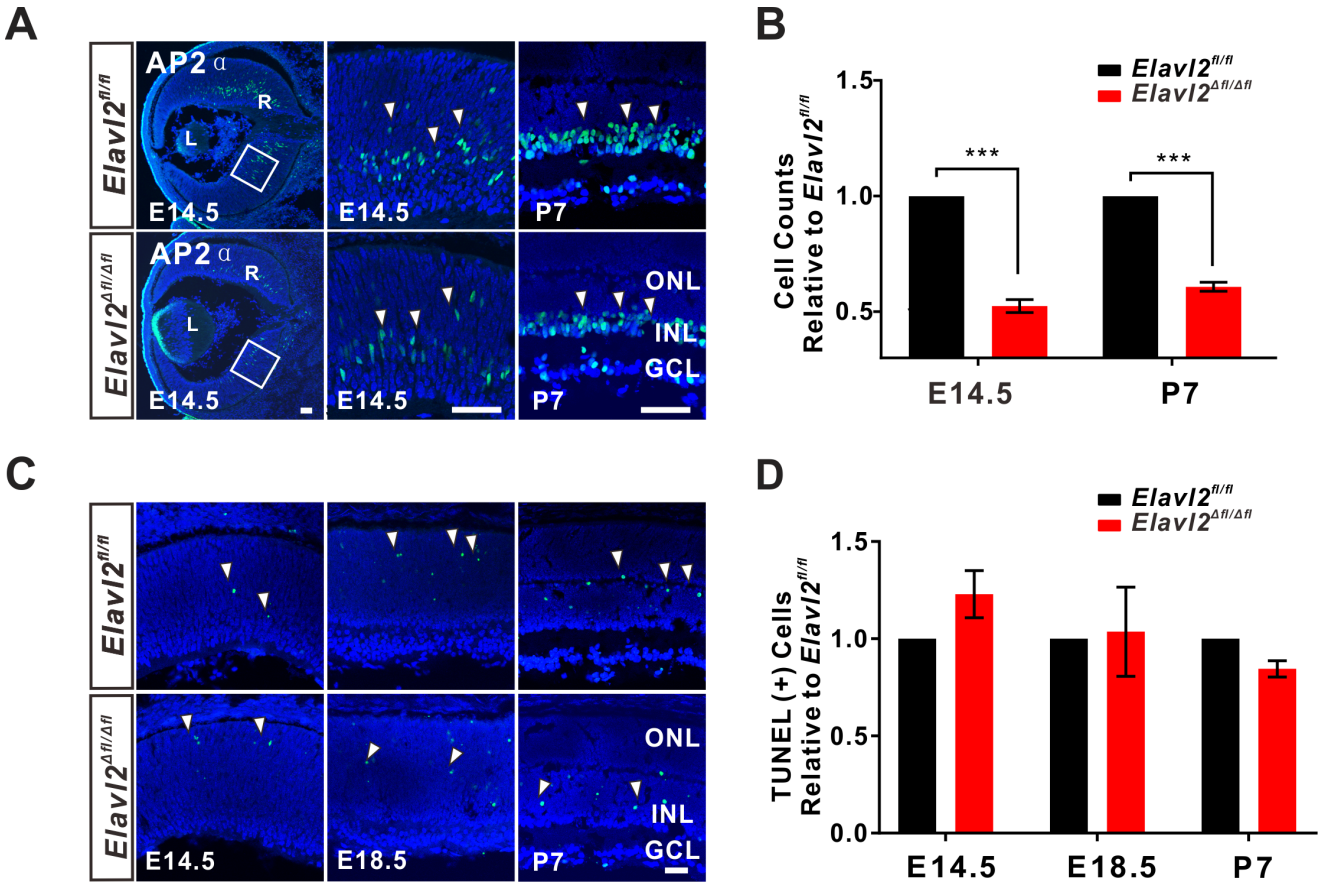

Figure 4. *Elavl2* deficiency alters the differentiation of ACs in the early stage of retinal development. **(A)** Immunostaining of retinal sections at E14.5 from *Elavl2*$^{fl/fl}$ and *Elavl2*$^{\Delta fl/\Delta fl}$ mice were double-immunostained with anti-AP2α antibody (*green*) and DAPI (*blue*). *Arrowheads* indicated the AP2α^{+} ACs. **(B)** Quantitation of cells that were immunoreactive for AP2α in E14.5 and P7 *Elavl2*$^{\Delta fl/\Delta fl}$ and the control retinas, and normalized to *Elavl2*$^{fl/fl}$ littermates. Results are presented as the mean ± SEM (n ≥ 3). **(C)** Retinal cross-sections of *Elavl2*$^{fl/fl}$ and *Elavl2*$^{\Delta fl/\Delta fl}$ mice, stained for TUNEL (*green*) and DAPI (*blue*). **(D)** Quantitation of TUNEL^{+} cells in E14.5, E18.5 and P7 *Elavl2*$^{\Delta fl/\Delta fl}$ and the control retinas, and normalized to *Elavl2*$^{fl/fl}$ littermates. Results are presented as the mean ± SEM (n ≥ 3). *Asterisks* indicate statistically significant differences between *Elavl2*$^{fl/fl}$ and *Elavl2*$^{\Delta fl/\Delta fl}$ mice. *P < 0.05, **P < 0.01, ***P < 0.001.

retinas, with a peak expression level at around E14.5, and progressively decreased and persisted at lower levels for up to P120 (Fig. 1N). These results were consistent with the previously study in the brain.[34]

We next performed immunofluorescent staining using antibodies against Elavl2 and double labeled with several cell type- and subtype-specific markers of retinal cells at P14 (around the mouse eye-opening day), to determine which of these cell types express Elavl2. We detected coexpression of Elavl2 in 68.9% ± 6.7% of the Pax6^{+} cell, a marker for amacrine, ganglion, and horizontal cells (Figs. 2A, 2K). Although colocalization with Elavl2 was determined in 79.8% ± 1.3% AP2α^{+} ACs, 17.7% ± 2.0% Rbpms^{+} RGCs, and 7.8% ± 1.8% Calbindin^{+} HCs in the INL, we observed rare Elavl2 expression in bipolar cells (BCs) and Müller cells (MGs) (Figs. 2B–2G, 2K). To further characterize the Elavl2^{+} ACs subtype, we assessed and observed that subsets of Elavl2^{+} ACs were GABA^{+} ACs (60.0% ± 3.8%) and GLYT1^{+} ACs (43.0% ± 0.5%) (Figs. 2H, 2I, 2K). Furthermore, Elavl2 was also expressed in a small population of CHAT^{+} (10.3 ± 0.9%; Figs. 2J, 2K) ACs, which was involved in the direction selectivity of RGCs.[35]

Conditional Ablation of *Elavl2* Leads to a Specific Reduction of ACs in Retina

To investigate the role of Elavl2 in the retina, we conditionally ablated *Elavl2* in retinal progenitors (Fig. 3A). The expression levels of *Elavl2* DNA (Fig. 3B) and mRNA

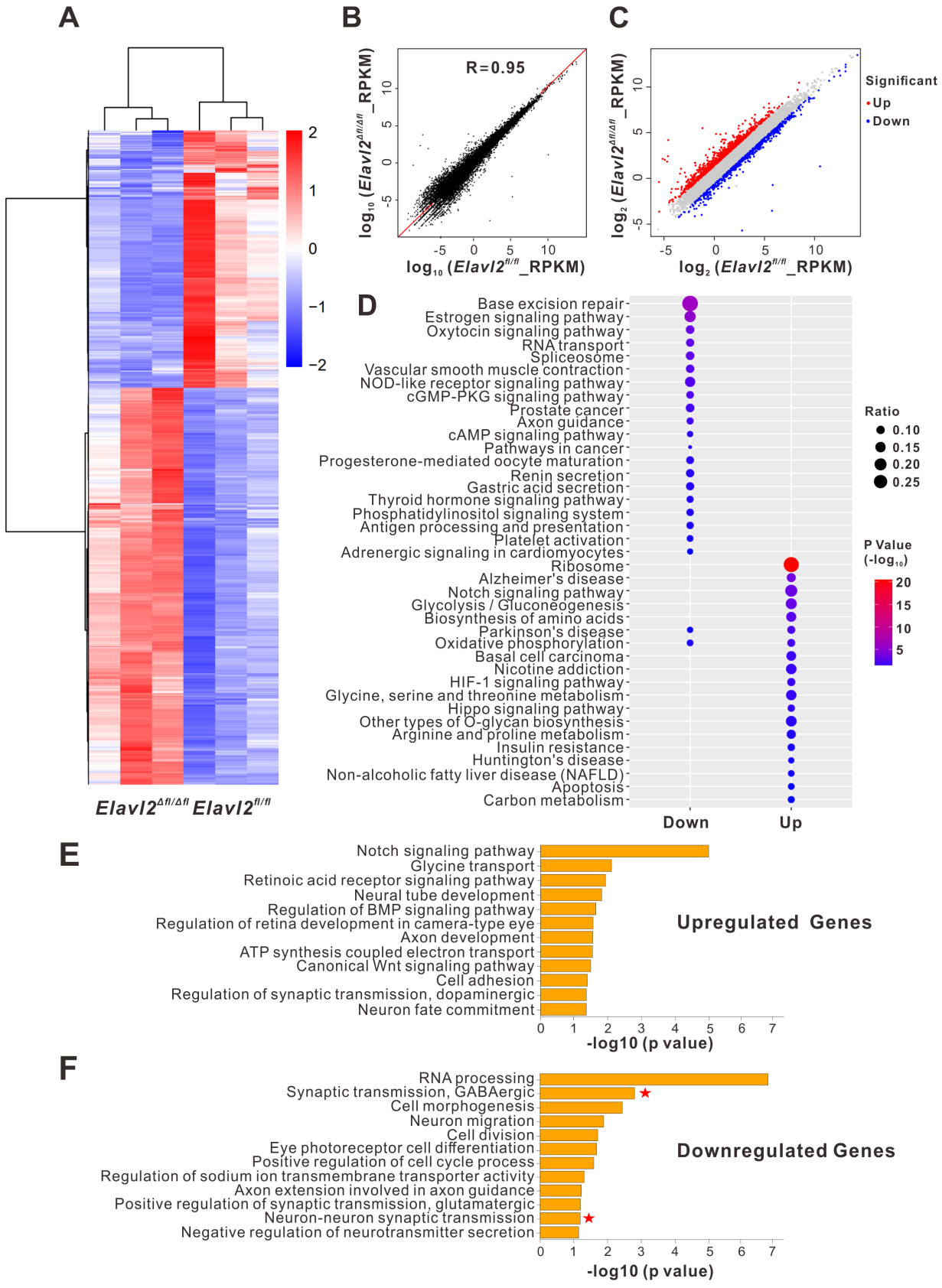

Figure 5. RNA-seq analysis reveals the differentially expressed genes in *Elavl2*$^{\Delta fl/\Delta fl}$ retinas at P6. **(A)** Cluster analysis presented a large group of significantly upregulated genes and a smaller group of significantly downregulated genes in the *Elavl2*$^{\Delta fl/\Delta fl}$ retinas. **(B)** Scatter plot of global gene expression profiles and the Spearman correlation coefficient was indicated. The levels of gene expression (reads per kilobase per million reads) were depicted in $\log_{10}$ scale. The diagonal line represented equal expression levels in the *Elavl2*$^{fl/fl}$ and *Elavl2*$^{\Delta fl/\Delta fl}$

Investigative Ophthalmology & Visual Science

retinas. **(C)** Scatter plot of significantly upregulated (*red*) and downregulated (*blue*) genes (fold change ≥ 2.0 and $P < 0.05$) between the *Elavl2*$^{fl/fl}$ and *Elavl2*$^{\Delta fl/\Delta fl}$ retinas. **(D)** Enriched KEGG pathways identified in the differentially expressed genes belonging to the *Elavl2*$^{\Delta fl/\Delta fl}$ retinas. **(E, F)** Gene ontology (GO) terms that related to the retina of upregulated **(E)** and downregulated **(F)** genes set in *Elavl2*$^{\Delta fl/\Delta fl}$ retinas compared to *Elavl2*$^{fl/fl}$ retinas. The *red stars* indicate the category in GO analysis closely related to our hypothesis.

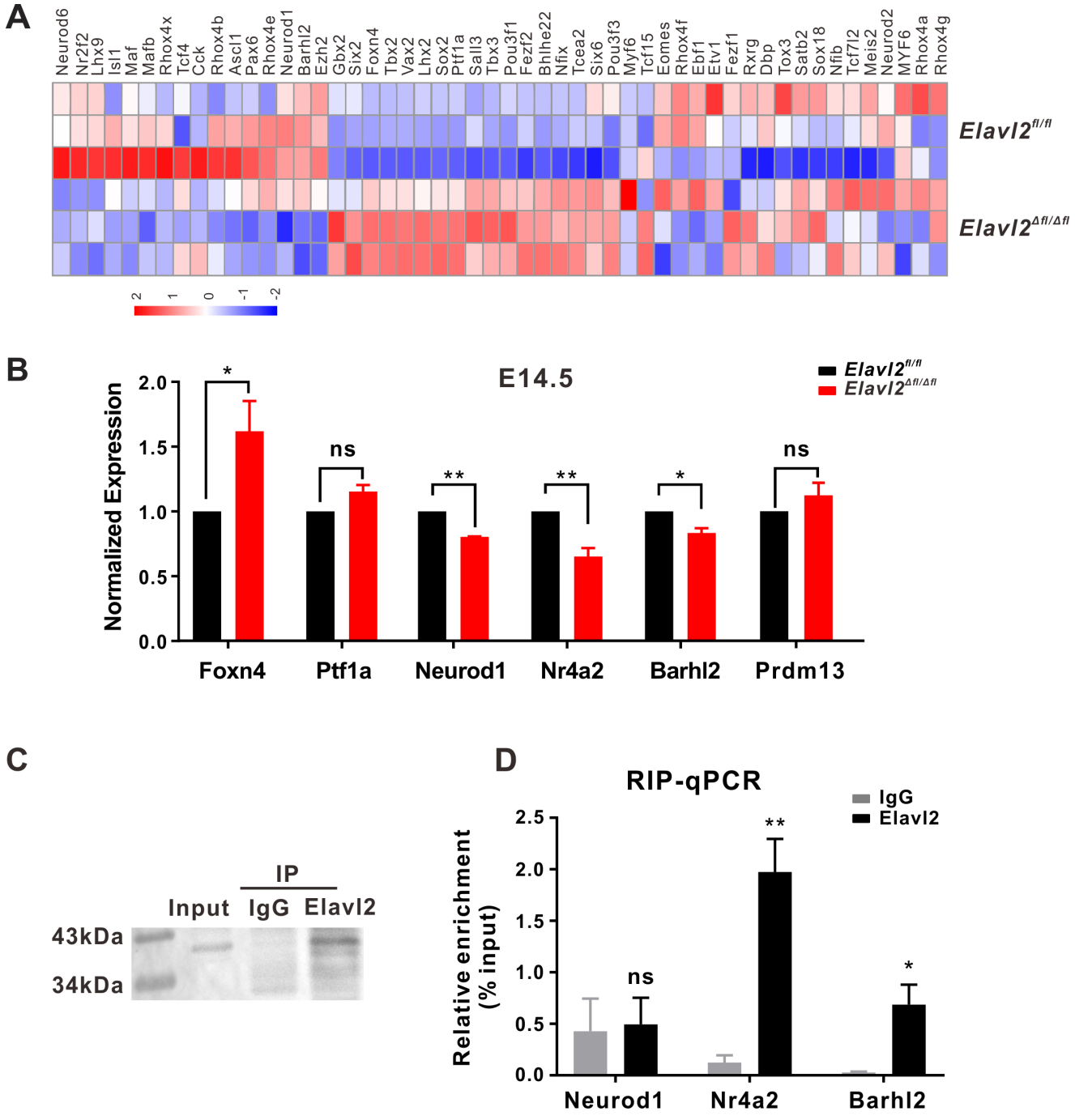

Figure 6. Elavl2 is involved in the differentiation of ACs during retinogenesis. **(A)** The heat map of expression levels for transcription factors (TFs) for ACs development in the retina. **(B)** The qRT-PCR analyses of the related TFs genes in *Elavl2*$^{fl/fl}$ and *Elavl2*$^{\Delta fl/\Delta fl}$ mice at E14.5. Results are presented as the fold expression relative to *Elavl2*$^{fl/fl}$ littermates, with *error bars* representing standard error of the mean (SEM, n ≥ 3). *Asterisks* indicate statistically significant differences between *Elavl2*$^{fl/fl}$ and *Elavl2*$^{\Delta fl/\Delta fl}$ mice. **(C)** Immunoprecipitation assay using anti-Elavl2 antibody in wild type retina. **(D)** The interaction between Elavl2 and Nr4a2, Barhl2 and Neurod1 mRNA in wild type retina based on RIP and qRT-PCR analyses. Results are presented as the mean ± SEM (n ≥ 3). *Asterisks* indicate statistically significant differences between Elavl2 and IgG. *$P < 0.05$, **$P < 0.01$, ns, no significance.

Investigative Ophthalmology & Visual Science

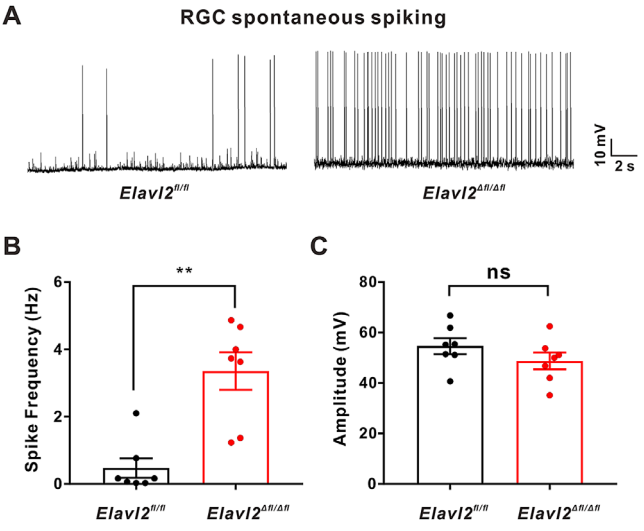

Figure 7. *Elavl2* deficiency increases spontaneous spike activity in RGCs at P30. **(A)** Spontaneous spike activity observed in RGCs in *Elavl2*$^{fl/fl}$ (left) and *Elavl2*$^{\Delta fl/\Delta fl}$ (right) retinas. **(B, C)** The mean spontaneous spiking frequency **(B)** and amplitude **(C)** in RGCs in *Elavl2*$^{fl/fl}$ (*black lines*) and *Elavl2*$^{\Delta fl/\Delta fl}$ (*red lines*) retinas. Results are presented as the mean ± SEM (n ≥ 7). *Asterisks* indicate statistically significant differences between *Elavl2*$^{fl/fl}$ and *Elavl2*$^{\Delta fl/\Delta fl}$ mice. *$P < 0.05$, **$P < 0.01$; ns, no significance.

(Fig. 3C) from different genotypes were measured to verify the reduction of *Elavl2* and the feasibility of the model in our study. To explore the consequences of *Elavl2* deficiency, the histology of the retinas were probed using immunohistochemistry and cell type-specific markers at P30. Although no significant changes were observed in optic nerve and retina cells types, including RGCs, BCs, HCs, MGs and photoreceptor cells, a notable decrease in AP2α^+ neurons in the INL and ganglion cell layer in *Elavl2*$^{\Delta fl/\Delta fl}$ retinas through quantifying the immunoreactive cells compared with *Elavl2*$^{fl/fl}$ retinas (Figs. 3D, 3E). These results were consistent with the qRT-PCR assay of specific retinal cell-related genes (Fig. 3F). In agreement with the loss of AP2α^+ neurons, the number of GABA$^+$ ACs and GlyT1$^+$ ACs were obviously reduced in *Elavl2*$^{\Delta fl/\Delta fl}$ retinas, when compared to the controls (Figs. 3G, 3H). However, there was no change of CHAT$^+$ ACs numbers in E*lavl2*$^{\Delta fl/\Delta fl}$ retinas (Figs. 3G, 3H).

Because ACs were born between E8 to P5 in the mouse retina,[36] we set about to quantify the number of ACs in *Elavl2*$^{\Delta fl/\Delta fl}$ on E14.5 and P7 to determine whether the reduction occurred in the early stage of retinal development. We found that consistent with the decreased ACs in developed retina (P30), the number of AP2α^+ ACs significantly decreased in developing retina (E14.5 and P7) (Figs. 4A, 4B). No more increased TUNEL$^+$ cells in *Elavl2*$^{\Delta fl/\Delta fl}$ retinas were observed, indicating that the loss of ACs was not resulting from ACs apoptosis (Figs. 4C, 4D).

Elavl2 Ablation Reduces ACs Differentiation Revealed by RNA-Seq Analyses

To further probe the mechanism and function of Elavl2 during retinogenesis, we carried out RNA-seq analysis to identify genes in *Elavl2*$^{\Delta fl/\Delta fl}$ retinas with differentially expression. This analysis yielded 1596 unique transcripts that displayed more than twofold change in their expression levels in *Elavl2*$^{\Delta fl/\Delta fl}$ retinas, of which 968 genes were upregulated, and 628 genes were downregulated respectively (Figs. 5A, 5C). Moreover, we performed enrichment analysis of these altered transcripts followed by visualization, which yielded the major clustered of KEGG pathway (Fig. 5D). To evaluate the effect of transcripts on the retinal development, we further calculated the gene ontology category, and which was enriched for neuron fate, retina development and synaptic transmission (Figs. 5E, 5F).

Previously, a series of TFs, including Foxn4, Ptf1a, Prdm13, Neurod1, Nr4a2 and Barhl2 were involved in the specification and differentiation of ACs.[10,14,17,37,38] We calculated the heatmap of TFs that involved in the specifying ACs fate during retinogenesis[39] (Fig. 6A). Consistent with what we observed in RNA-seq, the TF genes *Neurod1, Nr4a2* and *Barhl2* were declined in *Elavl2*$^{\Delta fl/\Delta fl}$ retinas using the qRT-PCR analysis (Fig. 6B), whereas the *Foxn4* was overexpressed. However, there was no change in the level of *Ptf1a* and *Prdm13* in *Elavl2*$^{\Delta fl/\Delta fl}$ retinas (Fig. 6B). To further detect the association of individual TFs mRNA with Elavl2, we performed RIP assay and isolated RNA species associated with Elavl2 in vivo. Surprisingly, Elavl2 was efficiently coimmunoprecipitated the Nr4a2 and Barhl2, but not Neurod1 or Foxn4 (Figs. 6C, 6D, Supplementary Fig. S2), suggesting that Elavl2 could directly interact with Nr4a2 and Barhl2 mRNA.

Increased Spontaneous Activity of RGCs in *Elavl2*-Deficient Mice

RGCs as the only output neurons of retina, transferring the signals directly to the brain. To better investigate whether the deficiency of *Elavl2* had an impact on the electrophysiological properties of RGCs, the spontaneous spike activity of RGCs was recorded in *Elavl2*$^{\Delta fl/\Delta fl}$ retinas by whole-cell patch-clamp recordings. Interestingly, we found the spiking frequency of RGCs in *Elavl2*-deficient mice exhibited almost sixfold higher than those in controls (Figs. 7A, 7B). However, the amplitude of the action potential in RGCs has no significant difference in *Elavl2*-deficient mice compared to the controls (Fig. 7C). Thus we hypothesized that Elavl2-dependent changes in the spontaneous spiking frequency was associated primarily with the changes in ACs, which could directly affect the activity of RGCs through the synaptic connections and neurotransmitters.

Impaired ERG Responses in *Elavl2*-Deficient Mice

To investigate the retina functions after *Elavl2* deficiency, ERG recordings were carried out in *Elavl2*-deficient mice with age ranging from P30 to P270. Representative waveforms for the scotopic ERG responses were presented in Figures 8A and 8B, with the decreased b-wave and OPs amplitudes in *Elavl2*-deficient animals. The amplitudes of b-wave that driven by the activity of Rod bipolar cells[40] showed an approximately 30% decrease in P30 and P120 *Elavl2*$^{\Delta fl/\Delta fl}$ mice, whereas the a-wave that associated with photoreceptor activity has no obvious changes in amplitudes compared to the age-matched controls during our observation time until nine months (Fig. 8D, Supplementary Fig. S3). In contrast, the implicit times of scotopic ERG a- and b-waves in *Elavl2*$^{\Delta fl/\Delta fl}$ mice were similar to the controls and underwent no significant changes at any stimulus strength (Fig. 8E, Supplementary Fig. S3). Moreover, consistent with the loss of ACs in *Elavl2*$^{\Delta fl/\Delta fl}$ mice, the amplitudes of OPs elicited

Investigative Ophthalmology & Visual Science

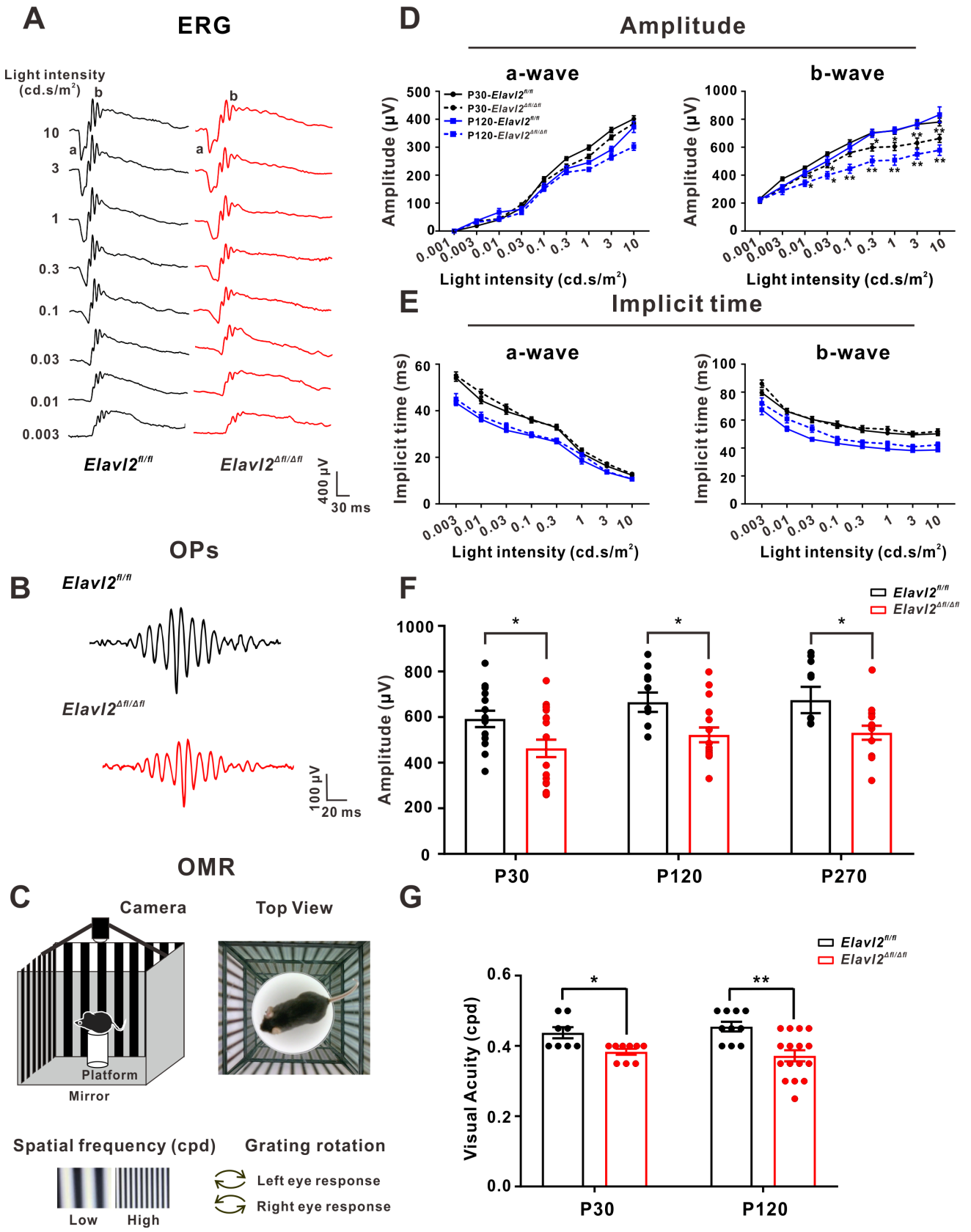

Figure 8. *Elavl2* deficiency causes deficit in electroretinogram (ERG) responses and visual acuity. **(A, B)** Representative waveforms (a-wave, b-wave, and OPs) from *Elavl2*$^{fl/fl}$ and *Elavl2*$^{\Delta fl/\Delta fl}$ mice recorded from ERG responses. The flash intensities used to elicit the responses are presented to the left. **(C)** Schematic illustrating the OMR testing apparatus and procedures. A mouse is placed freely on a platform, and the stimulus gratings are displayed on the LED screens surrounding the mouse (left). A mouse is tracking the moving grating on the top of the

Investigative Ophthalmology & Visual Science

platform (right). **(D, E)** The amplitudes **(D)** and implicit times **(E)** of the scotopic ERG a- and b-waves elicited from mice were recorded at P30 and P120. **(F)** Amplitudes of the scotopic OPs (3.0 cd. s/m^2) were quantified at P30, P120 and P270. **(G)** The visual acuity threshold in the scotopic OMR was measured from *Elavl2*$^{fl/fl}$ and *Elavl2*$^{\Delta fl/\Delta fl}$ mice aged at P30 and P120. Results are presented as the mean ± SEM (n ≥ 8). *Asterisks* indicate statistically significant differences between *Elavl2*$^{fl/fl}$ and *Elavl2*$^{\Delta fl/\Delta fl}$ mice. *P < 0.05, **P < 0.01.

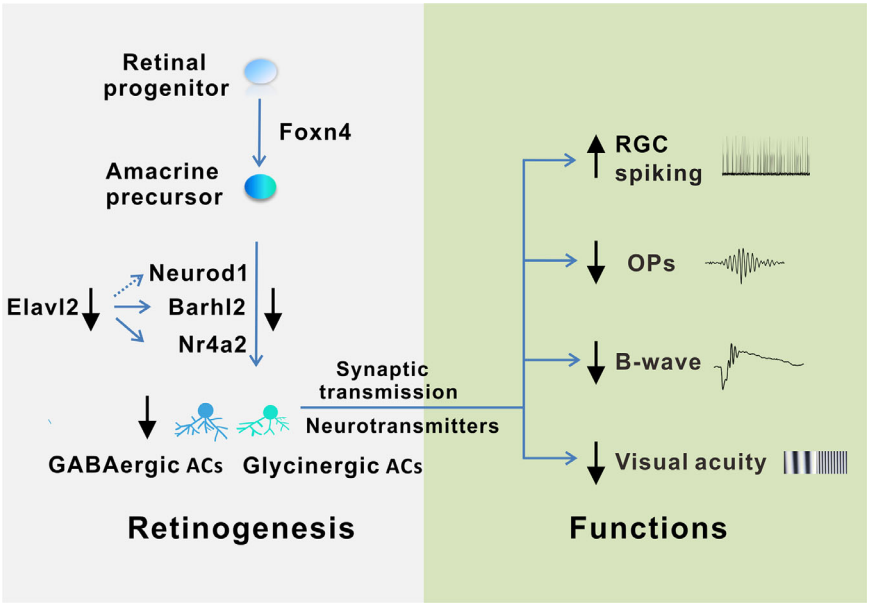

Figure 9. Summary diagram illustrating the hypothetical model for the Elavl2 function in ACs development and visual functions. Elavl2 could directly regulate the Barhl2 and Nr4a2 by binding to their mRNAs, together with indirectly modulate Neurod1 expression to modulate the differentiation of AP2a$^+$ ACs including GABAergic ACs and glycinergic ACs. Hence, in combination with the decreased ACs in *Elavl2*-deficient retinas, loss of *Elavl2* might disturb the balance of retinal neurotransmitters and cause increased the spontaneous activity of RGCs, decreased ERG response, as well as reduced visual acuity in the retina.

from mutant animals were decreased to approximately 30% of that of the controls at P30, P120, and P270, respectively (Fig. 8F).

Reduced Visual Acuity in *Elavl2*-Deficient Mice

The OMR is an ocular motor behavior induced by visual stimuli, which is currently used as a functional indicator of animal vision acuity.[30,41,42] To evaluate the effect of the deficiency in *Elavl2* on visual functions, OMR was carried out in mice (Fig. 8C). Obviously, the visual acuity in *Elavl2*$^{\Delta fl/\Delta fl}$ mice was declined at the age of P30 (Fig. 8G). Consistently, the impaired visual acuity was also recorded from homozygous animals in older mice at P120 (Fig. 8G).

Discussion

In the current study, we provide evidenced that Elavl2 is necessary for the development and functions of retina. Specific inactivation of *Elavl2* in the retina, leads to the decreased generation of AP2α^+ ACs including GABAergic and glycinergic ACs. Ultimately, *Elavl2*$^{\Delta fl/\Delta fl}$ mice presented the increased spontaneous activity of RGCs, reduced ERG response, together with impaired visual acuity.

In the mouse retina, Ptf1a and Prdm13 are important for differentiation of both GABAergic and glycinergic ACs.[15,43] Ablation of *Prdm13* leads to a significantly decreased in the number of CALBs$^+$ GABAergic or glycinergic ACs and represses the formation of Ebf3$^+$ ACs.[17,18] However, we could not determine a change in the level of Ptf1a and Prdm13 in *Elavl2*$^{\Delta fl/\Delta fl}$ retinas, suggesting other pathways independently controlled by Elavl2 to specify the subtypes of CALB$^+$ GABAergic and glycinergic ACs, and Ebf3$^+$ ACs. Additionally, it has been reported that Nr4a2 is both sufficient and necessary to confer AC precursors with the specification of ACs subtype, and inactivation of it would cause the loss of a subpopulation of GABAergic ACs.[21] The formation of glycinergic and GABAergic ACs were repressed notably in *Barhl2*-null retinas.[19] Similarly, the GABAergic ACs and glycinergic ACs were significantly decreased in *Elavl2*$^{\Delta fl/\Delta fl}$ retinas. Thus, in agreement with the previous studies, our experiments revealed that Elavl2 regulates the differentiation of GABAergic and glycinergic ACs through modulating the levels of Nr4a2 and Barhl2, with directly binding to their mRNAs.

Furthermore, compared with the controls, we found a decreased in the level of Neurod1 and Neurod4 in *Elavl2*$^{\Delta fl/\Delta fl}$ retinas, meanwhile, most of the specific Müller cells markers were upregulated using RNA-seq analysis (Supplementary Fig. S4). Some studies have reported that, ACs in the *Neurod1-Neurod4* double mutant retinas are completely missing while Müller cells increased.[44] In contrast, misexpression of *Neurod1* would suppress the Müller cells fate.[45] Thus, on the basis of the statistical results of Müller cells we did at P30, we speculated that the ablation of *Elavl2* may temporarily promote Müller cells formation through decreasing the level of Neurod1 and Neurod4,

Investigative Ophthalmology & Visual Science

and regulate the differentiation of ACs subtype. However, for further analysis, such as specifically labeling Elavl2^{+} ACs in *Elavl2*$^{\Delta fl/\Delta fl}$ retinas, it will be necessary to track the processing of the development and differentiation of ACs.

Interestingly, we detected the higher spontaneous RGCs activities and impaired ERG responses via electrophysiological studies in *Elavl2*$^{\Delta fl/\Delta fl}$ mice. The b-wave of scotopic ERG is largely driven by the activation of Rod bipolar cells,[40] whereas the OP is oriented in the laterally retinal cells associated with inhibitory ACs in visual processing in the retina.[46] It has been reported, $GABA_C$ receptors, located in axon terminals of bipolar cells, are likely to take participate in the regulation of the ERG b-wave because of a mechanism involving tonic GABA-induced Cl^- current in the retinal circuitry.[47] When the $GABA_C$ receptor antagonists were injected intravitreally in rats or mouse retina, the b-wave amplitudes were obviously reduced.[47,48] In the profiled transcriptomes analysis, ablation of *Elavl2* also reduced GABAergic synaptic transmission (Fig. 5F, star). Moreover, nElavls are required to control neuronal excitability by regulating neurotransmitter levels in neurons.[49] Elavl2 could modulate synaptic functions and play a key role in neurodevelopmental disorders.[50] Consequently, the dysfunction in *Elavl2*$^{\Delta fl/\Delta fl}$ retina is likely due to the ACs deficiency and causing the imbalance of inhibitory and excitatory neurotransmitter in the retina.

Together, during retinogenesis, Elavl2 could modulate the differentiation of GABAergic ACs and glycinergic ACs by binding to the target mRNAs (Nr4a2 and Barhl2), and indirectly regulating the level of Neurod1. Following the imbalance of neurotransmitters caused by the loss of ACs, deficiency of *Elavl2* could dramatically increase spontaneous RGCs activities, and ultimately disrupt the amplitude of ERG responses and visual acuity (Fig. 9). Thus our studies possibly reveal novel functions of Elavl2 in the retinal development and provide a new concept to further understand the neurological diseases caused by Elavl2 deficiency.

Acknowledgments

Supported by the National Key R&D Program of China (No. 2017YFE0103400) and the National Nature Science Foundation of China (No. 81800872).

Disclosure: **M. Wu,** None; **Q. Deng,** None; **X. Lei,** None; **Y. Du,** None; **Y. Shen,** None

References

1. Okano HJ, Darnell RB. A hierarchy of Hu RNA binding proteins in developing and adult neurons. *J Neurosci*. 1997;17:3024–3037.
2. Bronicki L, Jasmin B. Emerging complexity of the HuD/ELAVl4 gene; implications for neuronal development, function, and dysfunction. *RNA (New York, NY)*. 2013;19:1019–1037.
3. Yano M, Hayakawa-Yano Y, Okano H. RNA regulation went wrong in neurodevelopmental disorders: The example of Msi/Elavl RNA binding proteins. *Int J Dev Neurosci*. 2016;55:124–130.
4. Akamatsu W, Okano HJ, Osumi N, et al. Mammalian ELAV-like neuronal RNA-binding proteins HuB and HuC promote neuronal development in both the central and the peripheral nervous systems. *Proc Natl Acad Sci USA*. 1999;96:9885–9890.
5. Szabo A, Dalmau J, Manley G, et al. HuD, a paraneoplastic encephalomyelitis antigen, contains RNA-binding domains and is homologous to Elav and Sex-lethal. *Cell*. 1991;67:325–333.
6. Shibata M, Nakao H, Kiyonari H, et al. MicroRNA-9 regulates neurogenesis in mouse telencephalon by targeting multiple transcription factors. *J Neurosci*. 2011;31:3407–3422.
7. Kowalczyk T, Pontious A, Englund C, et al. Intermediate neuronal progenitors (basal progenitors) produce pyramidal-projection neurons for all layers of cerebral cortex. *Cereb Cortex (New York, NY: 1991)*. 2009;19:2439–2450.
8. Hicks EA, Zaveri M, Deschamps PA, et al. Conditional deletion of AP-2alpha and AP-2beta in the developing murine retina leads to altered amacrine cell mosaics and disrupted visual function. *Invest Ophthalmol Vis Sci*. 2018;59:2229–2239.
9. Yan W, Laboulaye M, Tran N, et al. Mouse retinal cell atlas: molecular identification of over sixty amacrine cell types. *J Neurosci*. 2020;40:5177–5195.
10. Xiang M. Intrinsic control of mammalian retinogenesis. *Cell Mol Life Sci*. 2012;70:2519–2532.
11. Cepko C. The roles of intrinsic and extrinsic cues and bHLH genes in the determination of retinal cell fates. *Curr Opin Neurobiol*. 1999;9:37–46.
12. Livesey F, Cepko C. Vertebrate neural cell-fate determination: lessons from the retina. *Nat Rev Neurosci*. 2001;2:109–118.
13. Li S, Mo Z, Yang X, et al. Foxn4 controls the genesis of amacrine and horizontal cells by retinal progenitors. *Neuron*. 2004;43:795–807.
14. Liu S, Liu X, Li S, et al. Foxn4 is a temporal identity factor conferring mid/late-early retinal competence and involved in retinal synaptogenesis. *PNAS*. 2020;117:5016–5027.
15. Hanotel J, Bessodes N, Thélie A, et al. The Prdm13 histone methyltransferase encoding gene is a Ptf1a-Rbpj downstream target that suppresses glutamatergic and promotes GABAergic neuronal fate in the dorsal neural tube. *Dev Biol*. 2014;386:340–357.
16. Chang J, Meredith D, Mayer P, et al. Prdm13 mediates the balance of inhibitory and excitatory neurons in somatosensory circuits. *Dev Cell*. 2013;25:182–195.
17. Watanabe S, Sanuki R, Sugita Y, et al. Prdm13 regulates subtype specification of retinal amacrine interneurons and modulates visual sensitivity. *J Neurosci*. 2015;35:8004–8020.
18. Goodson N, Nahreini J, Randazzo G, et al. Prdm13 is required for Ebf3+ amacrine cell formation in the retina. *Dev Biol*. 2018;434:149–163.
19. Ding Q, Chen H, Xie X, et al. BARHL2 differentially regulates the development of retinal amacrine and ganglion neurons. *J Neurosci*. 2009;29:3992–4003.
20. Mo Z, Li S, Yang X, et al. Role of the Barhl2 homeobox gene in the specification of glycinergic amacrine cells. *Development (Cambridge, England)*. 2004;131:1607–1618.
21. Jiang H, Xiang M. Subtype specification of GABAergic amacrine cells by the orphan nuclear receptor Nr4a2/Nurr1. *J Neurosci*. 2009;29:10449–10459.
22. Marquardt T, Ashery-Padan R, Andrejewski N, et al. Pax6 is required for the multipotent state of retinal progenitor cells. *Cell*. 2001;105:43–55.
23. Zagozewski JL, Zhang Q, Eisenstat DD. Genetic regulation of vertebrate eye development. *Clin Genet*. 2014;86:453–460.
24. Bolger A, Lohse M, Usadel B. Trimmomatic: a flexible trimmer for Illumina sequence data. *Bioinformatics (Oxford, England)*. 2014;30:2114–2120.

25. Dobin A, Davis C, Schlesinger F, et al. STAR: ultrafast universal RNA-seq aligner. *Bioinformatics (Oxford, England)*. 2013;29:15–21.
26. Liao Y, Smyth G, Shi W. FeatureCounts: an efficient general purpose program for assigning sequence reads to genomic features. *Bioinformatics (Oxford, England)*. 2014;30:923–930.
27. Wu J, Mao X, Cai T, et al. KOBAS server: a web-based platform for automated annotation and pathway identification. *Nucleic Acids Res*. 2006;34:W720–724.
28. Shen Y, Luo X, Liu S, et al. Rod bipolar cells dysfunction occurs before ganglion cells loss in excitotoxin-damaged mouse retina. *Cell Death Dis*. 2019;10:905.
29. Huang L, Yuan T, Tan M, et al. A retinography projection regulates serotonergic activity and looming-evoked defensive behaviour. *Nat Commun*. 2017;8:14908.
30. Prusky GT, Alam NM, Beekman S, et al. Rapid quantification of adult and developing mouse spatial vision using a virtual optomotor system. *Invest Ophthalmol Vis Sci*. 2004;45:4611–4616.
31. Jiang Z, Yue WWS, Chen L, et al. Cyclic-nucleotide- and HCN-channel-mediated phototransduction in intrinsically photosensitive retinal ganglion cells. *Cell*. 2018;175:652–664.e12.
32. Link B, Fadool J, Malicki J, et al. The zebrafish young mutation acts non-cell-autonomously to uncouple differentiation from specification for all retinal cells. *Development (Cambridge, England)*. 2000;127:2177–2188.
33. Bhatia B, Singhal S, Tadman DN, et al. SOX2 is required for adult human muller stem cell survival and maintenance of progenicity in vitro. *Invest Ophthalmol Vis Sci*. 2011;52:136–145.
34. Okano H, Darnell R. A hierarchy of Hu RNA binding proteins in developing and adult neurons. *J Neurosci*. 1997;17:3024–3037.
35. Elshatory Y, Everhart D, Deng M, et al. Islet-1 controls the differentiation of retinal bipolar and cholinergic amacrine cells. *J Neurosci*. 2007;27:12707–12720.
36. Voinescu PE, Kay JN, Sanes JR. Birthdays of retinal amacrine cell subtypes are systematically related to their molecular identity and soma position. *J Comp Neurol*. 2009;517(5):737–750.
37. Zhang X, Serb JM, Greenlee MHW. Mouse retinal development: a dark horse model for systems biology research. *Bioinf Biol Insights*. 2011;5:BBI–S6930.
38. Jin K, Xiang M. Transcription factor Ptf1a in development, diseases and reprogramming. *Cell Mol Life Sci*. 2019;76:921–940.
39. Siegert S, Cabuy E, Scherf B, et al. Transcriptional code and disease map for adult retinal cell types. *Nat. Neurosci*. 2012;15:487–495, S481–S482.
40. Leinonen H, Tanila H. Vision in laboratory rodents—tools to measure it and implications for behavioral research. *Behav Brain Res*. 2018;352:172–182.
41. Douglas RM, Alam NM, Silver BD, et al. Independent visual threshold measurements in the two eyes of freely moving rats and mice using a virtual-reality optokinetic system. *Vis Neurosci*. 2005;22:677–684.
42. Kretschmer F, Sajgo S, Kretschmer V, et al. A system to measure the Optokinetic and Optomotor response in mice. *J Neurosci Methods*. 2015;256:91–105.
43. Nakhai H, Sel S, Favor J, et al. Ptf1a is essential for the differentiation of GABAergic and glycinergic amacrine cells and horizontal cells in the mouse retina. *Development*. 2007;134:1151–1160.
44. Hatakeyama J, Tomita K, Inoue T, et al. Roles of homeobox and bHLH genes in specification of a retinal cell type. *Development (Cambridge, England)*. 2001;128:1313–1322.
45. Cherry TJ, Wang S, Bormuth I, et al. NeuroD factors regulate cell fate and neurite stratification in the developing retina. *J Neurosci*. 2011;31:7365–7379.
46. Wassle H. Parallel processing in the mammalian retina. *Nat Rev Neurosci*. 2004;5:747–757.
47. Wang J, Mojumder DK, Yan J, et al. In vivo electroretinographic studies of the role of GABAC receptors in retinal signal processing. *Exp Eye Res*. 2015;139:48–63.
48. Kapousta-Bruneau NV. Opposite effects of GABA(A) and GABA(C) receptor antagonists on the b-wave of ERG recorded from the isolated rat retina. *Vis Res*. 2000;40:1653–1665.
49. Ince-Dunn G, Okano HJ, Jensen KB, et al. Neuronal Elav-like (Hu) proteins regulate RNA splicing and abundance to control glutamate levels and neuronal excitability. *Neuron*. 2012;75:1067–1080.
50. Berto S, Usui N, Konopka G, et al. ELAVL2-regulated transcriptional and splicing networks in human neurons link neurodevelopment and autism. *Hum Mol Genet*. 2016;25:2451–2464.

Investigative Ophthalmology & Visual Science